

Modelling seismic time-lapse changes in the overburden and in the reservoir as a result of reservoir depletion.

Petar Vladov Angelov^{*,1}, Jesper Spetzler¹, Rob Arts^{1,2} and Kees Wapenaar¹

¹Delft University of Technology, Department of Geotechnology, The Netherlands

²TNO, Utrecht, The Netherlands

Summary

Variations in pressure (and saturation) at reservoir level over time influence not only the geomechanics of the reservoir, but also of the surrounding medium. Differences in the geomechanics bias the time-lapse seismic analysis. Using geomechanical and reservoir modelling it is possible to solve the forward problem and monitor the seismic attributes (travel time and amplitude) as a function of changes in the geomechanical model. This solution is then used for solving the inverse problem (i.e., finding the changes in the rock physics parameters over time from the time-lapse changes in the seismic response). Amplitude and travel time 4D changes, in the overburden and in the reservoir, should be monitored to achieve one accurate quantification of the time-lapse changes at the reservoir level.

Introduction

Stammeijer et al. (2004) and Hatchell et al. (2003) analysed the time shift differences in seismic data caused by compaction and changes in the stress field. They demonstrated that time shifts in the overburden could be larger than time shifts in the reservoir. We started by investigating the overburden effect using a synthetic geomechanical model, built with a finite element software package (“DIANA”). Using the relationships between stress and P-wave velocity for shales published by Wang (2002), it was possible to calculate the velocity variations in the overburden as a function of changes in the stress field. Applying the ray theory on our perturbed models we quantified the time shifts, for zero offset data, in the overburden as a result of injection. Our first results are published in Angelov et al. (2005). In this paper, we pursue our research where we model depletion instead of injection and investigate the near, mid and far offset time shifts as well. We also investigate the amplitude changes using the AVO (amplitude versus offset) analysis in anisotropic media. The effect of anisotropy is included under the assumption of weak anisotropy, (e.g., Thomsen, 2002). We built several geomechanical models with different elastic properties of the reservoir. To compute the time shifts for the different offsets to the top and bottom of the reservoir, we applied a ray perturbed theory (Snieder and Sambridge, 1992). The order of magnitude of the time shifts, and amplitude variations is depending on the elastic and geometrical properties of our model, as well as on the intensity of the depletion.

Geomechanical Modelling

We use the finite element software package (“DIANA”), to compute our geomechanical models. All the models are in a state of plane strain. We considered 2½D stress field modelling, applying a linear stress-strain relationship. The model consists of two parts: 1) reservoir and 2) surrounding medium (see Fig. 1). We work with a homogeneous surrounding medium for the reference case. Six models were compiled with different types of reservoirs. The reservoirs differed effectively in their values of the Young modulus, the Poisson ratio and density, with the surrounding medium remaining unchanged for all the different models. For each of the models, three different scenarios of depletion in the reservoir are simulated, with pore pressure decreases of 5, 10 and 15 MPa with respect to the initial effective stress of 25 MPa. More information about the modelling part can be found in Angelov et al. (2005). Using the geomechanical output of “DIANA”

	Surrounding medium		
Elastic parameters	$E_{sur}[GPa]$	ν_{sur}	$\rho_{sur}[kg/cm^3]$
	11.3	0.243	2319
	Reservoir		
Elastic parameters	$E_{res}[GPa]$	ν_{res}	$\rho_{res}[kg/cm^3]$
Model 1	7.901	0.164	1962
Model 2	7.545	0.163	1943
Model 3	7.205	0.162	1923
Model 4	6.881	0.162	1903
Model 5	6.571	0.161	1884
Model 6	6.274	0.160	1864

Table 1: The six different initial models used in the modelling part with the elastic parameters of the reservoir and surrounding medium.

and the stress-velocity relation of Wang (2002), we could calculate the travel time variations caused by changes in velocity and due to changes in physical distance (compaction). The maximum displacement is in the order of 27 cm, making the effect of displacement on the travel time attribute negligible.

Time shift and geometrical spreading factor

We applied the ray perturbed theory by Snieder and Sambridge (1992), to quantify the travel times as a result of production and overburden effect for P-waves. The

Overburden and reservoir 4D changes

ray path in the heterogeneous medium is decomposed into a reference and perturbed path. The reference ray is computed from the reference medium. The perturbed ray is estimated from the perturbed medium. Spetzler (2001) extended the ray perturbation theory of Snieder and Sambridge, to include the geometrical spreading factor. We generated results for zero, near, mid and far offset at the top and at the bottom of the reservoir.

Weak anisotropy

We make two different maps of the time shifts with and without the effect of anisotropy. To simulate weak anisotropy, we based our approach on the laboratory experiments of Wang (2002) and calculated the velocity field using the parameters for weak anisotropy given by Thomsen (2002)

$$V_P(\Theta) = V_P(0) \left[1 + \delta \sin^2 \Theta \cos^2 \Theta + \epsilon \sin^4 \Theta \right], \quad (1)$$

where Θ is the ray propagating angle, V_P is the velocity of compressional wave, δ and ϵ are Thomsen's parameters.

Amplitude variations

The time-lapse variations in the amplitude are calculated at the top and bottom interface of the reservoir. To compute the AVO we use the formulation given by Rüger (2002),

$$\begin{aligned} R_P(i) &= R_P^{ani}(i) + R_P^{iso}(i), \\ R_P^{ani}(i) &= \frac{1}{2}([\delta]) \sin^2(i) + \frac{1}{2}([\epsilon]) (\tan^2(i) - \sin^2(i)), \\ R_P^{iso}(i) &= \left(\frac{1}{2} \left(\frac{[V_P]}{\langle V_P \rangle} + \frac{[\rho]}{\langle \rho \rangle} \right) \right) + \\ &\quad \left(\frac{1}{2} \left(\frac{[V_P]}{\langle V_P \rangle} \right) \right) \sin^2(i) - \\ &\quad \left(2 \frac{\langle V_S \rangle^2}{\langle V_P \rangle^2} \left(2 \frac{[V_S]}{\langle V_S \rangle} + \frac{[\rho]}{\langle \rho \rangle} \right) \right) \sin^2(i) + \\ &\quad \left(\frac{1}{2} \left(\frac{[V_P]}{\langle V_P \rangle} \right) \right) (\tan^2(i) - \sin^2(i)). \end{aligned} \quad (2)$$

With $[]$ we denote the changes across the interface, $\langle \rangle$ is the average value across the interface, V_S is the shear velocity, ρ is density, i is the incident angle. R_P is the reflectivity, R_P^{iso} is the isotropic part and R_P^{ani} is the anisotropic part of the reflection response.

Results

Four different maps have been plotted to illustrate the overburden effect, (see Fig. 3 to Fig. 6). The maximum stress changes in the surrounding medium are concentrated on the interface between side burden and surrounding media. We investigated two different time

shifts: 1) the minimum time shift, which occurs at the top at the center of the reservoir, 2) the maximum time shift which occurs at the top nearby the edges of the reservoir.

Models	Δt [ms]							
	5[MPa]				15[MPa]			
	Z	N	M	F	Z	N	M	F
Model 1	0.3	0.3	0.3	0.3	0.9	0.9	1	1
Model 2	0.3	0.3	0.3	0.3	0.9	0.9	1	1.1
Model 3	0.3	0.3	0.3	0.4	1	1	1	1.1
Model 4	0.3	0.4	0.4	0.4	1	1	1.1	1.1
Model 5	0.3	0.4	0.4	0.4	1	1	1.1	1.2
Model 6	0.4	0.4	0.4	0.4	1.1	1.1	1.2	1.2

Table 2: Two way travel time shift (Δt) at the top at the center of the reservoir including the effect of anisotropy. The depletion in the reservoir pressure is indicated at the top of the columns. For each reservoir depletion, the time shifts for zero (Z), near (N), mid (M) and far (F) offsets are given.

Models	Δt [ms]							
	5[MPa]				15[MPa]			
	Z	N	M	F	Z	N	M	F
Model 1	0.5	0.5	0.4	0.3	1.5	1.4	1.2	1
Model 2	0.5	0.5	0.4	0.3	1.5	1.5	1.3	1
Model 3	0.5	0.5	0.4	0.4	1.6	1.5	1.3	1.1
Model 4	0.6	0.5	0.5	0.4	1.7	1.6	1.4	1.1
Model 5	0.6	0.6	0.5	0.4	1.8	1.7	1.4	1.2
Model 6	0.6	0.6	0.5	0.4	1.8	1.8	1.5	1.2

Table 3: Two way travel time shift (Δt) at the top at the edges of the reservoir including the effect of anisotropy. The notation is identical to Table 2.

Time-lapse changes in the overburden are influenced by the stress changes in the reservoir as a result of depletion. Since we use the relationship suggested by Wang (2002) to transform the changes in stresses into velocity time-lapse changes, every increase of effective stress changes in the reservoir will lead to an increase in velocity changes in the overburden. This trend is clearly seen in Fig 3 to Fig. 6, as well as in Table 2 and Table 3. After depletion in the reservoir pressure the reservoir presses to the sideburden. Because of this event we monitored high stress changes at the interface between the side burden and the reservoir. These stress changes depend on the contrast between the elastic properties of the reservoir and sideburdens. In Fig 3. to Fig. 6 we monitor a slight increase in time shift from models with ‘‘harder’’ elastic properties to models with ‘‘softer’’ elastic properties, (e.g., Table 1). We monitor the time shifts at the place with small stress changes and at the place with high stress changes concentration in the overburden, at the top of the reservoir. The time shift has been monitored for zero, near, mid and far offset. When the CMP is at the place with small time-lapse changes (the center of the reservoir), e.g., Table 2, time shift increases with increasing offsets. Therefore with increasing propagation angle, the wave travels closer to the zones with higher stress changes (near reservoir's edges). When the CMP is nearby the reservoir edges, we monitor a decrease in time shift from zero to far offset. In

Overburden and reservoir 4D changes

this case by increasing the angle of propagation, the ray paths decline away from the zone with higher time-lapse changes in the overburden. 7 to 17% from the absolute two way travel time time-lapse changes to the bottom of the reservoir are coming from the the overburden part of the model, (e.g., Table 4 and Table 5).

Different models	$\Delta t_{TOP}/\Delta t_{BOTTOM}$ [%]		
	5[MPa]	10[MPa]	15[MPa]
Model 1	7	8 ~ 7	9 ~ 8
Model 2	8 ~ 7	8 ~ 7	9 ~ 8
Model 3	8 ~ 7	8	9 ~ 8
Model 4	8	8	9 ~ 8
Model 5	8	8	9
Model 6	8	9	9

Table 4: Absolute values of the ratio (in percentage) between time shift to the top (Δt_{TOP}) and time shift (Δt_{BOTTOM}) to the bottom of the reservoir ($\Delta t_{TOP}/\Delta t_{BOTTOM}$). Travel times are calculated using the center of the reservoir as a CMP. The pressure depletion is indicated at the top of the columns.

Different models	$\Delta t_{TOP}/\Delta t_{BOTTOM}$ [%]		
	5[MPa]	10[MPa]	15[MPa]
Model 1	14 ~ 7	15 ~ 8	15 ~ 8
Model 2	14 ~ 7	15 ~ 8	16 ~ 8
Model 3	14 ~ 7	15 ~ 8	16 ~ 8
Model 4	15 ~ 8	16 ~ 8	17 ~ 9
Model 5	15 ~ 8	16 ~ 8	17 ~ 9
Model 6	16 ~ 8	17 ~ 9	17 ~ 9

Table 5: Absolute values of the ratio (in percentage) between time shift to the top (Δt_{TOP}) and time shift (Δt_{BOTTOM}) to the bottom of reservoir ($\Delta t_{TOP}/\Delta t_{BOTTOM}$). Travel times are calculated using the edges of the reservoir (325 m lateral distance from the edges) as CMPs. The notation is identical to Table 4.

Lastly a comparison between the variations in reflectivity (10 ~ 20 %) and geometrical spreading factor (~ 1 %), showed that the 4D effect of geometrical spreading factor is irrelevant (not illustrated in the figures).

Conclusions

From the results of our modelling, including geomechanical simulations and ray theory for all offsets, we conclude that the time shift as a result of production, by large pressure changes (15 MPa) can be detected (~ 2 ms). The production induced overburden effect, contributed up to 17 % in the time shift. This can bias the 4D seismic data analysis based on the changes in the travel time. The effect of anisotropy on the travel time, for this type of model is insignificant (~0.2 ms). The 4D effect on the geometrical spreading factor is insignificant compared to the changes in reflectivity. Field observations by Hatchell et al. (2003) do not corroborate all our modelling results so far. Hatchell et al. (2003) observe larger changes in travel times above the reservoir compared to changes in the reservoir. This is not in agreement with our modelling, e.g., Table 4 and Table 5. However, our

reservoir conditions have been quite different from these case studies. The next step will be to adapt our models such that they will be more representative for the case studies of Hatchell et al. (2003).

Acknowledgments

This research is supported by the Technology Foundation STW, applied science division of NWO and the technology program of the Ministry of Economic Affairs (grant DAR.5763). We thank Dr. Paul Hatchell (Shell) and Dr. John Verbeek (NAM) for suggesting the investigation of 4D overburden effects, as well as Dr. Bogdan Orlic (TNO) for his technical and scientific support.

References

- Angelov, P. V., Arts, R., Spetzler, J., and Wapenaar, K., 2005, Investigating the overburden effect on time-lapse seismic by geomechanical modelling: 67, EAGE.
- Hatchell, P., van den Beukel, A., Molenaar, M., Maron, K., Kenter, C., Stammeijer, J., van der Velde, J., and Sayers, C., 2003, Whole earth 4D:reservoir monitoring geomechanics: 73, Soc. Expl. Geophys., 1330–1333.
- Rüger, A., 2002, Reflection Coefficients and Azimuthal AVO Analysis in Anisotropic Media: Society of Exploration Geophysicists.
- Snieder, R., and Sambridge, M., 1992, Ray perturbation theory for traveltimes and ray paths in 3-d heterogeneous media.: Geophys. J. Int., **109**, 294–322.
- Spetzler, J., 2001, The effect of small-scale heterogeneity on the propagation of waves: Dissertation of Universiteit Utrecht.
- Stammeijer, J., van der Velde, J., Hatchell, P., van den Beukel, A., and Molenaar, M., 2004, Integrating 4D seismic and geomechanics: a case study.: 66, EAGE.
- Thomsen, L., 2002, Understanding seismic anisotropy in exploration and exploitation: Society of Exploration Geophysicists.
- Wang, Z., 2002, Seismic anisotropy in sedimentary rocks, part2: Laboratory data.: Geophysics, **67**, 1423–1440.

Overburden and reservoir 4D changes

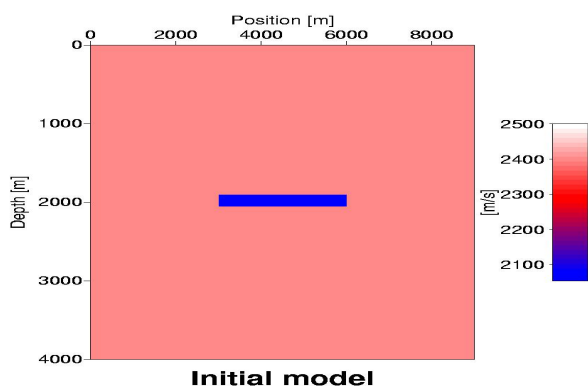


Fig. 1: Initial velocity model, i.e. reservoir (in blue) and surrounding medium.

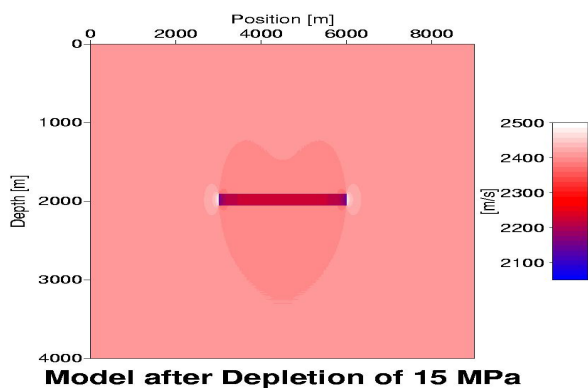


Fig. 2: The velocity model after depletion of 15 MPa. The model is developed with $2\frac{1}{2}$ D stress modelling

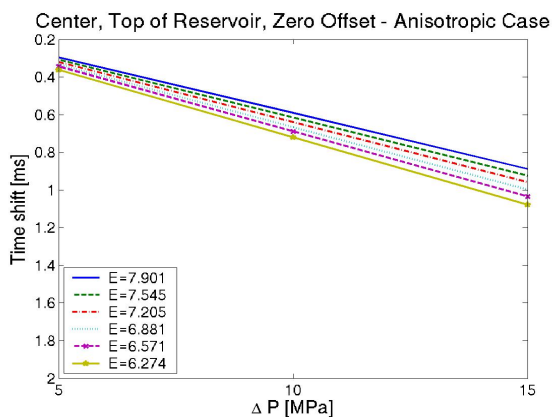


Fig. 3: The minimum of the time, which occurs at the center at the top of the reservoir. Zero offset case is considered. The effect of anisotropy has been included. A positive time shift corresponds to a longer traveltime.

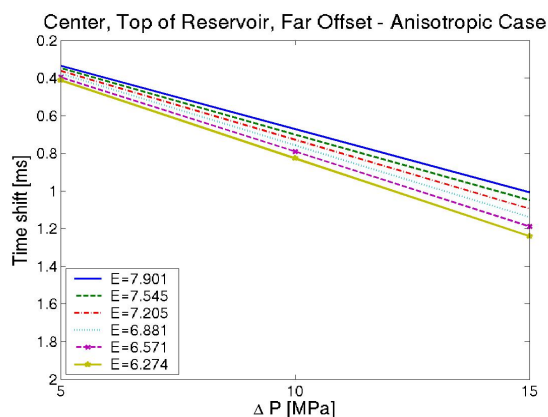


Fig. 4: The minimum of the time, which occurs at the center at the top of the reservoir. Far offset case is considered. The effect of anisotropy has been included. A positive time shift corresponds to a longer traveltime.

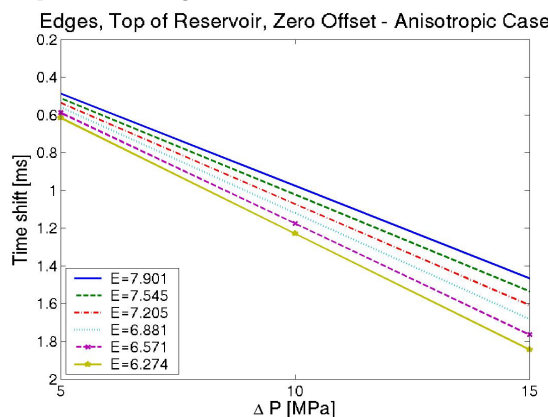


Fig. 5: The maximum of the time, which occurs at the edges at the top of the reservoir. Zero offset case is considered. The effect of anisotropy has been included. A positive time shift corresponds to a longer traveltime.

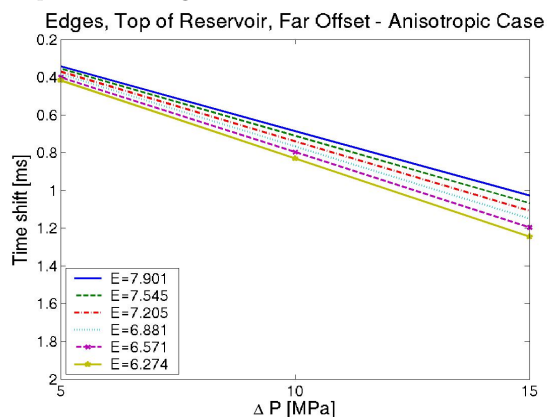


Fig. 6: The maximum of the time, which occurs at the edges at the top of the reservoir. Far offset case is considered. The effect of anisotropy has been included. A positive time shift corresponds to a longer traveltime.